Water Resources Research

RESEARCH ARTICLE
10.1029/2017WR021855

Geophysics-Based Contaminant Mass Discharge Quantification Downgradient of a Landfill and a Former Pharmaceutical Factory

Nicola Balbarini[1], Vinni Rønde[1], Pradip Maurya[2], Gianluca Fiandaca[2], Ingelise Møller[3], Knud Erik Klint[4], Anders V. Christiansen[2], Philip J. Binning[1], and Poul L. Bjerg[1]

[1]Department of Environmental Engineering, Technical University of Denmark, Lyngby, Denmark, [2]Department of Geoscience, Århus University, Århus, Denmark, [3]Geological Survey of Denmark and Greenland, Århus, Denmark, [4]Department of Environment, GEO, Denmark

Key Points:
- Surface direct current resistivity and induced polarization geophysical data can improve the interpolation of contaminant concentration data
- The geophysics-based method can improve estimation of contaminant mass discharge at large contaminated sites with low water-sample densities
- Surface geophysical data are affected by changes in inorganic species arising from a contaminant source or generated during biodegradation

Supporting Information:
- Supporting Information S1

Correspondence to:
N. Balbarini,
nbal@env.dtu.dk

Citation:
Balbarini, N., Rønde, V., Maurya, P., Fiandaca, G., Møller, I., Klint, K. E., et al. (2018). Geophysics-based contaminant mass discharge quantification downgradient of a landfill and a former pharmaceutical factory. *Water Resources Research*, *54*, 5436–5456. https://doi.org/10.1029/2017WR021855

Abstract Contaminant mass discharge is a commonly applied tool to evaluate the environmental impact of contaminated sites on water resources. At large contaminated sites with heterogeneous sources, such as landfills, the number of wells available is often not sufficient, leading to a high uncertainty of mass discharge estimates. In this study, we tackle the uncertainty of the contaminant mass discharge due to low sampling densities by interpolating limited water-sample data with the support of surface direct current resistivity and induced polarization geophysical data. The method relies on finding a conceptual link between the bulk conductivity imaged from geophysics and the contaminant concentrations. We investigate the link between (1) imaged bulk and electrical water conductivity, (2) water conductivity and conservative ionic species, (3) water conductivity and redox-sensitive species, (4) water conductivity and semipersistent organic species, and (5) water conductivity and biodegradable organic compounds. The method successfully identify similarities between the distribution of the bulk conductivity and chloride and pharmaceutical compounds in a landfill leachate plume and between the bulk conductivity data and benzene and chlorinated ethenes for a contaminant plume from a former pharmaceutical factory. Contaminant concentrations were interpolated through regression kriging, using geophysical data as the dependent variable. The distribution of concentration determined with the novel method showed a lower mean relative estimation error than the traditional method of kriging only contaminant concentration data. At large sites, the method can improve contaminant mass discharge estimates, especially if surface geophysical measurements are integrated in the site investigation at an early stage.

Received 15 SEP 2017
Accepted 9 MAY 2018
Accepted article online 24 MAY 2018
Published online 16 AUG 2018

1. Introduction

Large and heterogeneous contaminant sources, such as abandoned landfills (Bjerg et al., 2011; Cozzarelli et al., 2011) and former industrial production facilities (Bockelmann et al., 2003), require site investigations and long-term monitoring in order to assess the risk for the surrounding water resources and the environment. Surface-based geophysical electrical methods, such as direct current resistivity and induced polarization (DCIP), are particularly suitable for investigations at large contaminated sites, where many boreholes would be needed to obtain a sufficiently high sampling density. Resistivity methods have been successfully applied at landfill sites for plume detection (e.g., Chambers et al., 2006; Frid et al., 2017; Maurya et al., 2017; Ogilvy et al., 2002), because the landfill leachate plume often has a high inorganic ion content (Christensen et al., 2001). Maurya et al. (2017) was able to show a qualitatively relationship between the resistivity in the plume and the ionic strength measured in the boreholes, but no quantitative relationship was presented. Laboratory and field studies have been able to identify the degradation of petroleum hydrocarbons (e.g., Aal et al., 2004; Allen et al., 2007; Atekwana & Atekwana, 2010), because production of charged species, such as organic acids and alkalinity, increases the DC signal. Nevertheless, the DC resistivity method does not allow discrimination between high salinity of groundwater and formations with a low resistivity (e.g., clay).

In a porous medium, electrical conduction occurs through the fluid that fills the interconnected pore spaces (electrolytic bulk conduction) and through the electrical double layer of the sediment grains (surface conduction; e.g., Lesmes & Frye, 2001). The induced polarization method, which provides information on both the bulk and

surface conduction/polarization (e.g., Binley, 2015), can help in distinguishing changes in salinity from those due to lithology (e.g., Weller et al., 2013). Therefore, it has been increasingly applied for contaminated site investigations, for example, mapping the extent of landfill waste (e.g., Dahlin et al., 2010; Gazoty et al., 2012a; Wemegah et al., 2017) and lithological properties (e.g., Gazoty et al., 2012b; Johansson et al., 2016; Kemna et al., 2004).

Contaminant mass discharge is a commonly applied method to evaluate the environmental impact of contaminated sites on groundwater quality (Cai et al., 2011; Guilbeault et al., 2005; Kübert & Finkel, 2006; Troldborg et al., 2010, 2012). At field sites, the contaminant mass discharge can be estimated downstream from the source at control planes that cover the entire width and depth of a plume and are orientated perpendicular to the groundwater flow direction. The uncertainty of the contaminant mass discharge estimate is related to the density of the sampling grid, to the heterogeneity of the flow field, and to the contaminant concentration field along the control plane (Kübert & Finkel, 2006; Troldborg et al., 2012). At large contaminated sites, characterized by high source heterogeneity such as landfills, it is often not economically feasible to install the number of multilevel wells required to ensure a sufficiently dense sampling grid (Troldborg et al., 2010).

To tackle the limitation of the control plane approach, surface geophysical surveys have been suggested as a useful tool to integrate point measurements (Rubin & Hubbard, 2005). Nevertheless, methods have yet to be developed to integrate geophysical data in the estimation of contaminant mass discharge.

This study aims to develop a novel method for describing the distribution of contaminant concentration by integrating geophysical and chemical data using regression kriging. Specifically, DCIP data were used for imaging the spatial distribution of the bulk conductivity, after removing the effect of the surface conductivity (Fiandaca et al., 2018b; Maurya et al., 2018). When combined with additional knowledge on groundwater flow, the geophysics-based method should be beneficial compared to the traditional approach of using only concentration data from multilevel samplers (termed the concentration-based approach) for contaminant mass discharge estimation from large and heterogeneous sources. The two methods are tested and compared at two field sites, representing contaminant plumes with different sizes and chemical characteristics. At Grindsted landfill, a wide leachate plume (600 m wide and 60 m deep) with high concentrations of inorganics and pharmaceutical compounds was investigated. Then, at Grindsted stream, a shallow plume (80 m wide and 12 m thick) was studied, which contained high concentrations of chlorinated ethenes and BTEX (benzene, toluene, ethylbenzene, and xylenes) and a low concentration of inorganics (relative to the landfill site). At both sites a geological model has been developed and the hydraulic properties of the aquifers have been characterized as a part of the study.

2. Field Sites

2.1. Grindsted Landfill Site: Source, Geology, and Hydrogeology

The landfill (Figure 1a) covers an area of 10 ha, where 300,000 t of waste were disposed between 1930 and 1977. In the northern part of the landfill, 85,000 t of waste originating from a former pharmaceutical factory was deposited, creating a hotspot area and a downgradient plume. The plume has very high concentrations of pharmaceutical compounds, mainly sulfonamides and barbiturates (Holm et al., 1995; Kjeldsen et al., 1998a, 1998b), with the highest measured concentrations in recent monitoring being 67,850 and 5,307 μg/L of sulfonamides and barbiturates, respectively.

The landfill is located in an area with primarily sand deposits within the upper ∼80 m of the subsurface. From ground surface at ∼40 m above sea level (asl) to ∼30 m asl, a Quaternary meltwater layer of mainly medium to coarse grained and gravelly sand is present. The sediments are deposited on an outwash plain located west of the Late Weichselian Main Stationary Line. At ∼30 to ∼–40 m asl a Miocene sand succession belonging to the Odderup Formation is present. The Miocene sand is deposited in a coastal and lagoonal environment (Rasmussen et al., 2010). The Miocene sand is mostly fine grained with two successions of mostly medium grained quartz sand from 20 to 10 m asl and from −15 to −40 m asl. The sand successions have intercalated mica clay and lignite beds of up to 1 m thickness. Four thin clay beds can be seen in the geological samples from the boreholes. Below −40 m asl, a thick and regionally extended clay layer of the Arnum Formation underlines the unconfined aquifer (Heron et al., 1998).

A control plane (L–L′) employed to estimate the contaminant mass discharge (Figure 1b) was placed downgradient from the Grindsted landfill, approximately perpendicular to the groundwater flow. Seven wells

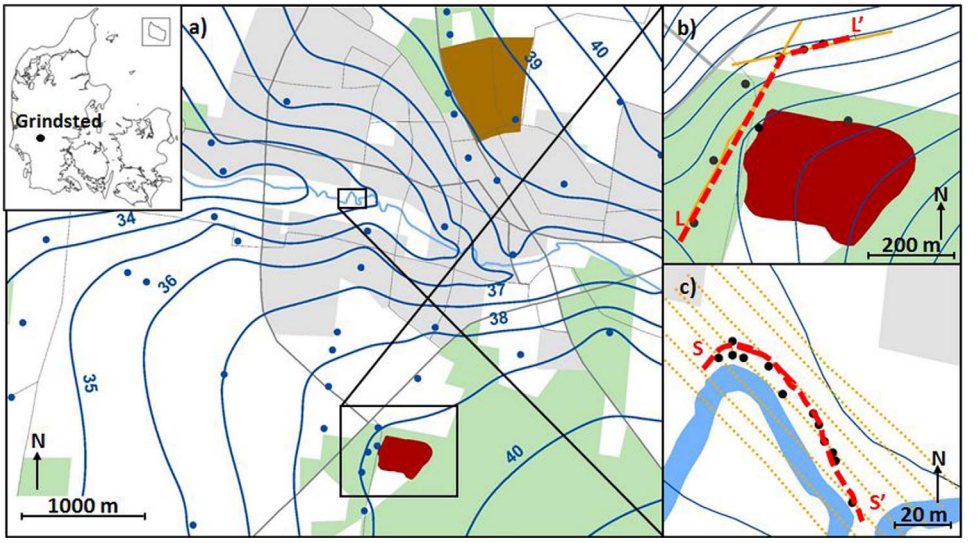

Figure 1. (a) Map of Grindsted town (grey shading and inset map of Denmark) showing the two investigated areas (clear boxes): the landfill and stream sites. The factory site (light brown) is located north of the stream site and the landfill site (dark red) is located south of the stream. The equipotential lines (m asl) are indicated by the blue lines, originated by water head data collected at wells marked by blue dots. The location of the control plane (red dashed lines), DCIP profiles (orange dots), and multilevel sampling wells (black dots) are shown in (b) for the landfill and (c) for the stream site. Note the differences in scales for Figures 1b and 1c.

with multilevel 1–2 m long screens were placed along the control plane, equipped with a total of 20 screens (Maurya et al., 2017). The concentrations measured in each screen of barbiturates and sulfonamides are shown in supporting information Figure S1. The concentration of chloride was measured in 14 screens, out of the 20 available. The geometric mean of the hydraulic conductivities estimated by slug tests performed in all screens was 1.7×10^{-4} m/s with a variance of the log-normalized hydraulic conductivities (ln *K*) of 0.9.

2.2. The Grindsted Stream Site: Source, Plume, Geology, and Hydrogeology

At the Grindsted stream site (Figure 1c), the upper contaminant plume originating from the former pharmaceutical factory enters the stream from the north with high concentrations of BTEX (mainly benzene) and chlorinated ethenes including the degradation products (*cis*-1,2-dichloroethene, *cis*-DCE, and vinyl chloride; Rønde et al., 2017; Sonne et al., 2017). The highest measured concentrations are 1,744 μg/L of benzene, 5,571 μg/L of *cis*-DCE, and 5,160 μg/L of vinyl chloride.

The stream site is characterized by the presence of clay-rich deposits in the 15 m immediately below ground surface, underlain by a sand-dominated succession. Thin layers (∼1–2 m thickness) of postglacial sand are present within the stream valley, while thin peat layers are present and in the stream plain. The postglacial stream valley is cut into meltwater sand deposited on the outwash plain formed at the Late Weichselian Glacial maximum. Here the meltwater sand is ∼4–6 m thick and consists of mostly medium coarse sand. Locally, the remains of a Saalien sand till of up to 4 m thickness and older meltwater deposits of ∼2–3 m thickness are preserved. The top of the Miocene succession is located at 10–12 m depth at ∼25 m asl and consists of a ∼5 m thick mica clay and lignite succession with interbedded sand. Below the clay-rich top layer of the Miocene succession the geology is dominated by mica and quartz sand as at the landfill site.

Most of the highest contaminant concentrations are located in the upper meltwater sand. The focus of this study is on the upper aquifer, which is in close hydraulic contact with the stream (Balbarini et al., 2017). The control plane (S–S′) employed to estimate the contaminant mass discharge at the Grindsted stream is located perpendicular to the groundwater flow and parallel to the stream meander (Figure 1c). Twelve multilevel drive point (0.1 m long) screens were placed along the control plane, providing a total of 58 data points (Rønde et al., 2017). The concentration of vinyl chloride, *cis*-DCE, and benzene in the control plane are shown in supporting information Figure S2.

Hydraulic conductivity values measured using slug tests by Rønde et al. (2017) are available at 53 locations along the profile. The geometric mean of the hydraulic conductivity was 5.6×10^{-5} m/s in the two upper freshwater formations, 1.8×10^{-4} m/s in the Quaternary meltwater sand, and 4.3×10^{-5} m/s in the lower Quaternary sand till and Miocene layers. The variances of ln K were 3.4, 0.6, and 4.4, respectively for the freshwater formations, Quaternary sand, and the lower sand till and Miocene layers (Rønde et al., 2017).

3. Methodology

First, the methods for collecting the geophysical, geological, and contaminant concentration data are presented. Then, the geophysics-based method and concentration-based method for contaminant mass discharge are described, followed by the error and uncertainty analysis used to compare the two methods.

3.1. Direct Current Resistivity and Induced Polarization (DCIP)

The direct current (DC) and induced polarization (IP) method is used to investigate the spatial distribution of the electrical resistivity and charge storage capacity (the polarization) of the subsurface. The IP signal can be measured either in the frequency domain, as frequency-dependent complex resistance, or in the time domain, as a voltage decay response when the medium is excited by a square current pulse (as in this study).

The combined resistivity and polarization properties of the medium can be expressed in the frequency domain in terms of a complex conductivity (σ^*) as the sum of two current paths (e.g., Lesmes & Frye, 2001). One is the electrolytic bulk conduction (σ_{bulk}), which is the conduction that takes place through the fluid that fills the interconnected pore spaces, and the other is the complex surface conduction (σ^*_{surf}), which comprises both the surface conduction and the surface polarization of the electrical double layer formed at solid-fluid interface (through the real part σ'_{surf} and the imaginary part σ''_{surf}, respectively):

$$\sigma^*(f) = \sigma_{bulk} + \sigma^*_{surf}(f, \sigma_w) = \frac{\sigma_w}{F} + \sigma'_{surf}(f, \sigma_w) + i\sigma''_{surf}(f, \sigma_w) \tag{1}$$

where f is the excitation frequency, i is the imaginary unit and in the second equality the bulk conductivity σ_{bulk} is linked to the electrical water conductivity σ_w, and the formation factor F through Archie's law (Archie, 1942):

$$\sigma_{bulk} = \frac{\sigma_w}{F} \tag{2}$$

In equation (1) the dependence of σ'_{surf} and σ''_{surf} on the excitation frequency f and the water conductivity σ_w is explicitly stated. Furthermore, Weller et al. (2013) identified a strong linear relationship between σ'_{surf} determined from multisalinity resistivity measurements and σ''_{surf} measured with IP at a frequency of about 1 Hz:

$$\sigma''_{surf} = l \cdot \sigma'_{surf} \tag{3}$$

with $l = 0.042 \pm 0.022$ (dimension less). From equation (1), the total DC conductivity (σ_0) can be expressed as the sum of the bulk conductivity and the real part of the surface conductivity at zero frequency:

$$\sigma_0 = \frac{\sigma_w}{F} + \sigma'_{surf}(f = 0, \sigma_w) \tag{4}$$

Equation (4) clarifies that in media with high surface conduction, as clays and tills, the DC resistivity alone is not an ideal proxy for the water conductivity, which is the property of interest in this study. Weller et al. (2013) compared the true formation factor determined from multisalinity experiments to the formation factor estimated using a single salinity measurement ignoring surface conductivity (i.e., as $F = \frac{\sigma_w}{\sigma_0}$) and correcting for surface conductivity through equation (3) (i.e., as $F = \frac{\sigma_w}{\sigma' - \sigma''_{surf}/l}$). While the estimations of formation factor obtained ignoring the surface conductivity presented a systematic bias, the estimations obtained using equation (3) were scattered around the 1:1 line and closer to the true formation factor (with average deviation almost halved from 0.303 to 0.174 decades). However, a perfect correction was not achieved, as evidenced also by the high error on the factor l of equation (3). In a similar way, in this study the IP data are used to estimate the surface conductivity and bulk conductivity terms separate from measured conductivity, as explained in details in the inversion section.

3.1.1. Data Acquisition and Processing

The geophysical data used in this study are part of two more extensive geophysical surveys carried out at the landfill (Maurya et al., 2017) and stream site (Maurya et al., 2018). In this study, only the two geophysical profiles along the contaminant mass discharge control plane were used (orange lines in Figure 1b). The profiles are 600 and 400 m long (Figure 1b) and were acquired using 5 m electrode spacing. In Maurya et al. (2018), the induced polarization method is used to image the water conductivity and the hydraulic permeability at the stream site, and to help the construction of the geological model. Of the 14 profiles shown in Maurya et al. (2018), seven parallel profiles acquired with smaller electrode spacing (i.e., 2 m) are presented in this study. The data were collected using 64 electrodes with 2 m in-line spacing and 7 m intraline spacing, covering an area of 126 $\times$ 42 m^2 (Figure 1c).

The DCIP measurements were carried out using the Terrameter LS instrument (www.guidelinegeo.com) with the gradient array (Dahlin & Zhou, 2006). Full-waveform IP data were recorded at high sampling rate (1 kHz at landfill site and 3.75 kHz at stream site) with on-time $T_{on}=4$ s and off-time $T_{off}=4$ *s*. Full-waveform data were processed following the processing algorithm described by Olsson et al. (2016), for harmonic denoising and background drift removal. Processed data were gated using 36 logarithmically spaced time windows, in the time interval from 1 ms to 4 s. Resistivity and gated IP data (IP decays) were imported into Aarhus workbench software for manual data processing, in order to remove outliers (single gates or entire decays), caused by factors such as poor electrode contact or inductive effects at early-times.

3.1.2. Inversion

DC and full-decay IP data are inverted using the 2-D inversion algorithm presented by Fiandaca et al. (2013), with an accurate description of transmitter waveform and the receiver transfer function for an unbiased estimation of the spectral parameters (Fiandaca et al., 2012). The inversion model space consists of a parameterization of the complex conductivity of equation (1), defined in each cell of the 2-D model. The forward response and the Jacobian are computed in frequency domain over a set frequencies and transformed in time domain through a superposition of step responses computed by a fast Hankel transform, as described in Johansen and Sørensen (1979) and Fiandaca et al. (2013).

In this study, the complex conductivity is modeled as a reparameterization of the Cole-Cole model (Pelton et al., 1978), which is expressed in conductivity form as (e.g., Tarasov & Titov, 2013)

$$\sigma^*(f)=\sigma_0\cdot\left[1+\frac{\boldsymbol{m}_0}{1-\boldsymbol{m}_0}\cdot\left(1-\frac{1}{1+(\boldsymbol{i}2\pi\boldsymbol{f}\tau_\sigma)^{\boldsymbol{C}}}\right)\right] \tag{5}$$

where σ^* is the complex conductivity, σ_0 is the DC conductivity, $\boldsymbol{m}_0$ is the intrinsic chargeability, τ_σ is the relaxation time, C is the frequency exponent, f is the frequency, and i is the imaginary unit. In the Cole-Cole model, the real part of the complex conductivity increases with frequency, while the imaginary part reaches a maximum $\sigma''_{\max}$ at frequency $f={}^1/_{2\pi\tau_\sigma}$ (Figure 2).

Fiandaca et al. (2018a) have shown that the $\boldsymbol{m}_0$ and C parameters are strongly correlated in the inversion of IP data, and suggest reparameterization of the Cole-Cole model to improve parameter resolution, for instance by using the maximum imaginary conductivity $\sigma''_{\max}$ as the inversion parameter instead of $\boldsymbol{m}_0$. Furthermore, by enforcing the proportionality between σ'_{surf} and σ''_{surf} of equation (3) at the frequency $f={}^1/_{2\pi\tau_\sigma}$, it is possible to define the Bulk and (maximum) Imaginary Conductivity (BIC) Cole-Cole reparameterization (Fiandaca et al., 2018b; Maurya et al., 2018) as follows:

$$\boldsymbol{m}_{\boldsymbol{BIC}}=\left\{\sigma_{bulk},\sigma''_{\max},\tau_\sigma,C\right\} \tag{6}$$

Using the BIC reparameterization, the inversion retrieves, cell by cell in the 2-D model, the bulk conductivity σ_{bulk} (disentangled from the surface conductivity σ'_{surf}), together with the maximum imaginary conductivity $\sigma''_{\max}$ and the classic Cole-Cole parameters τ_σ and C. Again, the quality of the disentanglement of σ_{bulk} from σ'_{surf} depends on the effectiveness of equation (3), and a perfect disentanglement of bulk and surface conduction cannot be expected. Furthermore, the variability of the proportionality between σ'_{surf} and σ''_{surf} of equation (3) with frequency is not discussed in Weller et al. (2013). Enforcing the proportionality at the frequency $f={}^1/_{2\pi\tau_\sigma}$ is a conservative choice; in this way the ratio between the surface imaginary conductivity and real conductivity never exceeds the factor of equation (3). In contrast, enforcing the proportionality at $f=1$ Hz would imply a ratio well above *1* at the peak frequency $f=1/2\pi\tau_\sigma$ for models with $\tau_\sigma \gg 1$. Figure 2a

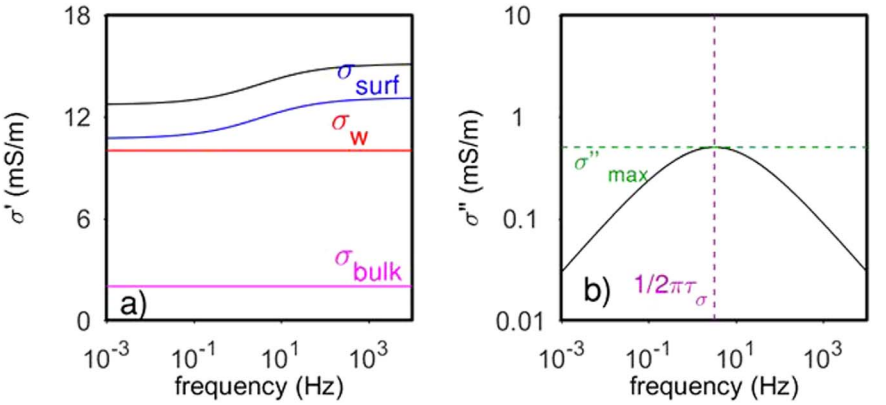

Figure 2. Spectrum of the Cole-Cole model. (a) real conductivity σ' (black curve), obtained as the sum of the bulk conductivity σ_{bulk} (magenta curve) and the surface real conductivity σ'_{surf}. The water conductivity value σ_w with formation factor $F = 5$ is also shown. (b) Imaginary conductivity σ''. The model parameters, in terms of the BIC parameterization (equation (6)), are defined as $\sigma_{bulk}=2$ mS/m, $\sigma''_{max}=0.5$ mS/m, $\tau_\sigma=0.05$ s, and $C=0.5$. Figure from Maurya et al. (2018).

shows σ_{bulk}, σ'_{surf} and the total real conductivity $\sigma'=\sigma_{bulk}+\sigma'_{surf}$ for the BIC model defined as $\sigma_{bulk}=2\frac{\text{mS}}{\text{m}}$, $\sigma''_{\text{max}}=0.5\frac{\text{mS}}{\text{m}}$, $\tau_\sigma=0.05$ s, and $C=0.5$, together with the water conductivity σ_w (computed assuming $F=5$).

Finally, the depth of investigation (DOI) of the inversions is computed parameter by parameter along the 2-D sections following Fiandaca et al. (2015).

3.2. Water Sampling and Chemical Analysis

At the landfill site, water samples were collected from all screens and analyzed for major cations and anions, sulfonamides, and barbiturates. The wells and sampling methods are described by Maurya et al. (2017). Samples for major ions were filtered (0.45 μm) and all samples were stored on dry ice in the field until analyses. The analytical methods are described for ions by Maurya et al. (2017), and for pharmaceutical compounds by Sonne et al. (2017). At the stream site, sampling and chemical analysis for major cations and anions and chlorinated ethenes are reported by Rønde et al. (2017) and Sonne et al. (2017).

3.3. Contaminant Mass Discharge Estimation

The contaminant mass discharge *CMD* (kg/yr) through a control plane can be calculated as

$$CMD = \sum_{n=1}^{N} C_n \cdot q_n \cdot A_n \tag{7}$$

where C_n is the contaminant concentration at section position n (mg/L), q_n is the groundwater flux normal to the plane in section n (m/d), and A_n is the area of section n (m^2; Kübert & Finkel, 2006; Li & Abriola, 2009; Mackay et al., 2012). One meter long quadratic sections were used at the landfill site and 0.1 m long quadratic sections were used at the stream site. The location of the control planes at the sites is shown in Figure 1.

In equation (7), the variation of the contaminant mass discharge across the control plane is described by the spatial distribution of the contaminant concentration (C_n) and of the groundwater flux (q_n). In this study, the focus is on providing a method for describing the spatial distribution of the contaminant concentration. The Grindsted landfill field site can be assumed to be mildly heterogeneous, since the variance of ln K is less than 1 (Bohling et al., 2012). Thus, a constant groundwater flux of 14.6 m/yr (based on the hydraulic gradient and the geometric mean hydraulic conductivity) was assumed for the entire plane. At the Grindsted stream, the contaminant plume core is located in the Quaternary sand layer, where the mean hydraulic conductivity is highest and the variance of the ln K is less than 1, again indicating a mild heterogeneity. The layers above and below the Quaternary sand show greater geological heterogeneity, but since both the mean hydraulic conductivity and the contaminant concentrations are much lower compared to the Quaternary sand layer, variations in the groundwater flow have a small impact on the contaminant mass discharge calculation. Hence, a constant groundwater flow velocity of 106 m/yr (based on direct groundwater velocity

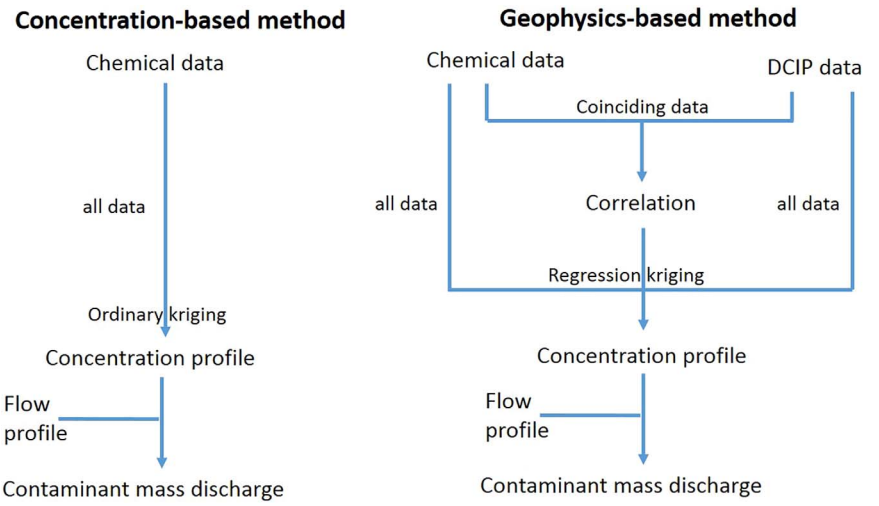

Figure 3. Concept for the contaminant mass discharge estimation methods: the contaminant concentration-based method and the geophysics-based method.

measurements, Rønde et al., 2017) is assumed for the entire control plane at the stream site. The effect of the constant groundwater flow velocity assumption on the contaminant mass discharge calculation is discussed in section 5.

3.4. Determination of the Contaminant Concentration Profile

A schematic figure describing the concentration-based and geophysics-based methods is shown in Figure 3. In the concentration-based method, the concentration data points were interpolated using ordinary kriging.

In the geophysics-based method, in order to benefit from the information provided by the DCIP, the chemical concentration data were interpolated using regression kriging. This kriging method is used when the estimated variable (e.g., the contaminant concentration), sampled at few locations, is correlated with an auxiliary variable (e.g., the imaged bulk conductivity from DCIP), sampled at many locations (Hengl, 2009; Hengl et al., 2007; Matheron, 1973; McBratney et al., 2003; Odeh et al., 1995).

In regression kriging, the weighted average of auxiliary variables measured at location s_0 is used to predict the target variable, accounting for the residuals:

$$\widehat{z}(s_0)=\sum_{k=0}^{p}\widehat{\beta}_k\cdot q_k(s_0)+\sum_{i=1}^{n}\lambda_i\cdot e(s_i) \tag{8}$$

where p is the number of auxiliary variables, $\widehat{\beta}_k$ are the estimated drift model coefficient, $q_k(s_0)$ are the measurements of the auxiliary variables at location s_0, $e(s_i)$ are the residuals (i.e., the difference between the simulated and the observed values of the target variable) at location s_i, $\widehat{z}(s_0)$ is the predicted value of the target variable at an interpolated location s_0, n is the number of observations, λ_i are the weights, and $z(s_i)$ is the observation at location s_i. In order to ensure a value of the auxiliary variable at the interpolated locations, the imaged bulk conductivity from DCIP was kriged using ordinary kriging. A comparison of the location of the values of bulk electrical conductivity values provided by the DCIP data inversion and the location of the screens for water samples is provided in supporting information Figures S3 and S4 for the Grindsted landfill and stream site, respectively. The use of the imaged bulk conductivity from DCIP methods to describe the distribution of the contaminant concentrations is investigated for locations where both variables are available, see section 3.5. All kriging methods used in this paper were implemented in R software (version 3.4.3) applying exponential variogram models.

3.5. Evaluation of Predicted Contaminant Concentrations

The contaminant mass discharge and the corresponding relative error are calculated for the geophysics-based and the concentrations-based methods. The method with the lowest error is preferable. The relative contaminant mass discharge estimation error can be calculated as

$$\text{Relative error} = \frac{|CMD - \widehat{CMD}|}{\widehat{CMD}} \quad (9)$$

where CMD is the estimated contaminant mass discharge and $\widehat{CMD}$ is the true mass discharge. Since the true mass discharge is not known, the contaminant mass discharge calculated using only some of contaminant concentration data is compared with the "true" estimation made using the full data set containing all measured contaminant concentrations. For each selected number of samples, 1,000 simulations of contaminant concentrations randomly chosen from the original data set were performed. The number of simulations was selected in order to balance the need for reliable outcomes and a realistic computational time (e.g., Kübert & Finkel, 2006; Schwede & Cirpka, 2010). The assumption that the contaminant mass discharge calculated using all contaminant concentrations can act as the true value is limited by the uncertainty of the estimation.

The relative uncertainty of the contaminant mass discharge is calculated as

$$\text{Relative uncertainty} = \frac{s(CMD)}{\mu(CMD)} \quad (10)$$

where $s(CMD)$ is the standard deviation and $\mu(CMD)$ is the mean value of the contaminant mass discharge estimation (Schwede & Cirpka, 2010). The uncertainty is determined for both the geophysics-based and the contaminant concentration-based methods for each set of 1,000 simulations characterized by the same sample density.

The error and uncertainty analysis are performed at the Grindsted landfill site for chloride and barbiturates at the Grindsted stream site for vinyl chloride. The analysis is conducted using different sample densities (stream site: ranging from 0.06 to 0.015 samples/m^2, equivalent to 58 and 14 data points, respectively; landfill site: ranging from 0.0003 to 0.0001 samples/m^2, equivalent to 14 and 5 data points, respectively) to describe the change in relative contaminant mass discharge error as a function of the sample density. The lower sample density analyzed (0.0001 samples/m^2) is much lower than the minimum sample density considered by Troldborg et al. (2012) of 0.02 samples/m^2. The initial sample density at the landfill site is 0.0003 samples/m^2 which, if applied at the stream site, would include only one sample. Thus, a direct comparison of the two sites with the same sampling density is not possible.

3.6. Dependence of Bulk Electrical Conductivity on Groundwater Composition

The electrical water conductivity depends on the concentration of ions in the water, i.e., the electrical water conductivity and ionic strength are positively correlated (Appelo & Postma, 2005). This provides a link between the bulk conductivity imaged through the DCIP data and the concentration of ionic compounds in groundwater, as has previously been described for geophysical mapping of landfill leachate plumes rich in inorganic compounds (e.g., Chambers et al., 2006; Frid et al., 2017; Maurya et al., 2017; Ogilvy et al., 2002).

3.6.1. Ionic Conservative Compounds and Semipersistent Organic Compounds

Ionic conservative compounds are anions such as bromide and chloride released from the contaminant source and following groundwater flow pathways. These compounds can be used as indicators of the contaminant plume. Similarly, persistent or semipersistent xenobiotic organic compounds with high water solubility, low octanol/water partition constant, and low degradability can also be used as indicators of the contaminant plume. Therefore, the concentration distribution of semipersistent xenobiotic organic compounds is similar to the concentration distribution of inorganic plume indicators, when released from the same source area. An example of semipersistent xenobiotic organic compounds is that of the pharmaceutical compounds found at Grindsted landfill (Holm et al., 1995; Kjeldsen et al., 1998b).

3.6.2. Effects of Biogeochemical Processes on Bulk Electrical Conductivity

In contaminant plumes, and especially in landfill leachate plumes, biogeochemical processes, related to biodegradation of dissolved organic carbon and corresponding redox processes can affect the concentration of organic and inorganic species. Relevant redox processes include depletion of dissolved electron acceptors (oxygen, nitrate, and sulfate) and formation of dissolved ionic and nonionic metabolic by products such as manganese (Mn^{2+}), iron (Fe^{2+}), and methane (see supporting information Table S1 for an overview of the electron donors, electron acceptors, and metabolic by-products). A sequence of redox zones can be linked to the concentration of redox-sensitive species along the contaminant plume, as described by Christensen et al. (2000) and demonstrated for the Grindsted landfill leachate plume by Bjerg et al. (1995). The

changes in the concentration of ionic species due to the redox processes (e.g., nitrate, manganese, iron, and sulfate) can cause changes in the electrical water conductivity and thereby bulk conductivity (or resistivity) according to Archie's law. Here we explore the link between the electrical water conductivity and the redox-sensitive species in order to investigate whether distribution of redox species can support the contaminant distribution in the control plane.

The distribution of chlorinated ethenes in a contaminant plume can be affected by reductive dechlorination, where tetrachloroethene (PCE) and trichloroethene (TCE) are transformed to DCE, mainly *cis*-DCE, and vinyl chloride (Badin et al., 2016; Chambon et al., 2013). The chlorinated ethenes act as electron acceptors, hence their degradation does not affect redox conditions and redox-sensitive species. However, their distribution and the ratio of compounds in a plume is, among other things, highly dependent on the redox conditions. In order for reductive dechlorination and generation of vinyl chloride from *cis*-DCE to occur, strongly reducing conditions (iron reducing to methanogenic) are required in the aquifer. Strongly reducing conditions are indicated by high concentrations of dissolved iron, low sulfate concentrations, and/or production of methane (Christensen et al., 2000). As previously described, the distribution of electrical water conductivity can potentially be used as an indicator of the distribution of redox-sensitive species or even redox conditions in the plume. If the electrical water conductivity is affected by the distribution of redox-sensitive species and the redox processes, then the distribution of water electrical conductivity may be similar to the distribution of chlorinated ethenes generated during reductive dechlorination. This is investigated at Grindsted stream site where high concentrations of chlorinated ethenes, particularly the metabolites vinyl chloride and *cis*-DCE, are found in the control plane.

3.6.3. Statistical Analyses

Principal Component Analysis was used to quantitatively examine relationships among the redox-sensitive parameters in the contaminant plume at the Grindsted stream site. Water samples upgradient and downgradient the control plane (Figure 1), as well as water samples at the control plane were included in the analysis. In order to detect significant relationships between the water samples, Hierarchical Cluster Analysis (SIMilarity PROFile analysis, SIMPROF $p < 0.05$) was applied. The statistical analyses were performed in PRIMER (Pedersen et al., 2006). Based on these analyses (supporting information Table S3), a main part of the contaminant plume characterized by highly reduced conditions (iron reducing to methanogenic conditions) was identified, and this became the focus area of the work presented in this paper.

Multiple regression analysis (supporting information Table S6) was performed using Microsoft Excel (2016) to examine the relationship between major ions and water electrical conductivity at both sites. Similarly, regression analyses were performed between water electrical conductivity and selected organic contaminants. All statistical analyses included *F* test and estimation of the coefficient of determination.

4. Results

In the following section, the results of the geophysical data collection and inversion are presented. Then, the electrical conductivity is compared with the lithological stratification and the electrical water conductivity. The geophysics-based method and the concentration-based method are applied at the landfill site and at the stream site. Error and uncertainty analyses for the two methods are provided at both field sites.

4.1. Imaging of Bulk Conductivity and Geologic Model

Figure 4 shows an example of BIC inversion along the second DCIP profile (from the north) of the stream site (Figure 1c). The total data misfit of the inversion is $\chi = 1.7$. Figure 4d represents the pseudosection of IP misfit (the χ value) over the entire decays, and Figure 4e shows three representative measured decays with error bars and corresponding fit. The total DC conductivity (Figure 4b) is retrieved from the BIC inversion parameters (Maurya et al., 2018, equation 13) and differs significantly from the bulk conductivity (Figure 4a), especially in the areas of high σ''_{max} values (Figure 4c), corresponding to the clay/till layers.

Figure 5 represents the geological models and the imaged bulk conductivity values along the control planes LL′ and SS′ (Figure 1) at the landfill and stream sites. The geological models were built using the methods of Maurya et al. (2018), making use of the lithological data, water conductivity and hydraulic head observed in boreholes, the imaging results of the IP survey, in terms of σ_{bulk}, σ_0, σ''_{max}, and IP-derived hydraulic permeability sections. Figure 5 shows that the distribution of bulk conductivities

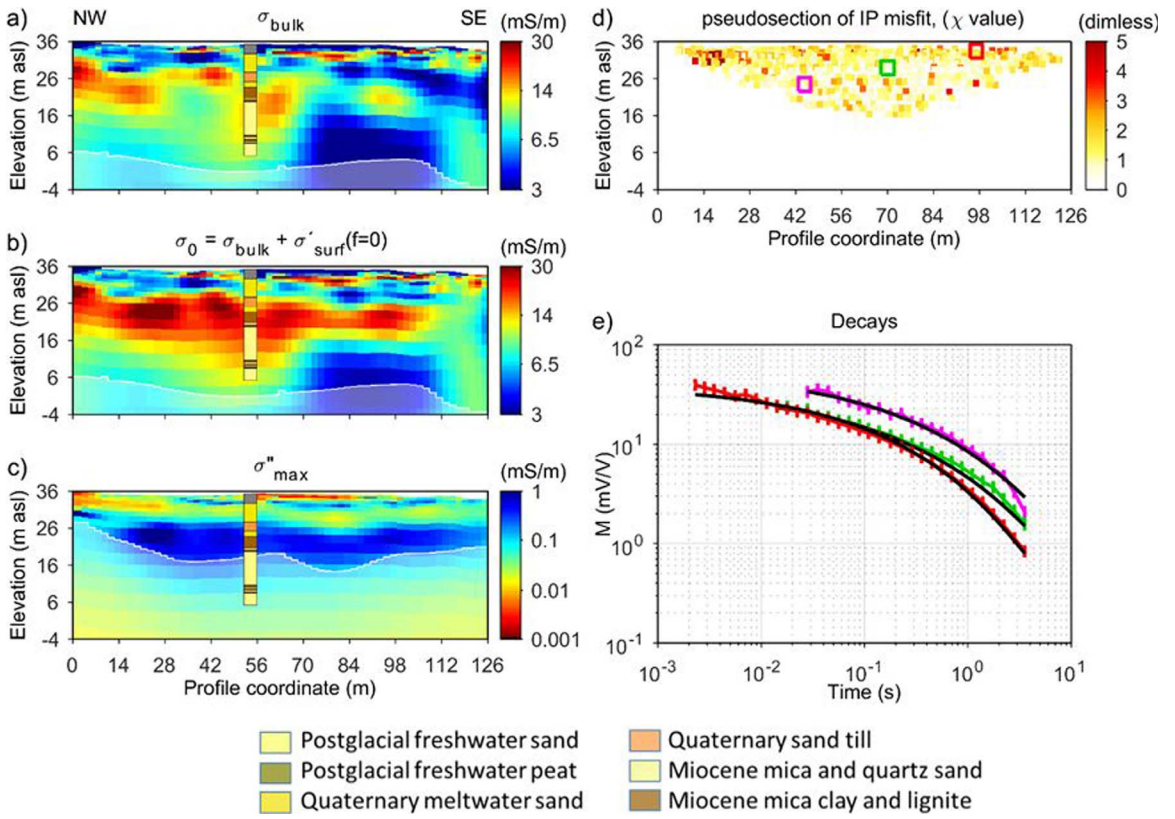

Figure 4. BIC inversion of the second DCIP profile (from the north) of Figure 1c. (a) Bulk conductivity section. (b) DC conductivity section, computed from the BIC parameters. (c) Maximum imaginary conductivity section. (d) Pseudo section of IP misfit, computed as χ value over the entire decays. (e) Examples of measured IP decays with error bars (colored lines, from the positions highlighted by the squares with corresponding colors in Figure 4d) and data fits (black lines). In Figures 4a–4c, the lithological information from a borehole near the profile is shown in color coding, while the depth of investigation by white color fading. Modified from Maurya et al. (2018).

cannot be explained by the lithological stratification and, thus, the water electrical conductivity plays an important role.

4.2. Determination of the Formation Factor by Use of Archie's Law

The bulk electrical conductivity, imaged with surface DCIP, depends on the electrical water conductivity, from water samples, as described by Archie's law (equation (2)). For the two field sites, the imaged bulk conductivity and the electrical water conductivity are linearly correlated, as shown in Figure 6. The inverses of the slopes of the regression lines are the formation factors, according to Archie's law. Since the Grindsted landfill and the Grindsted stream sites have similar geological properties, the sites have similar formation factors of 4.5 and 5.1, respectively. However, the coefficient of determination at the landfill site ($R^2 = 0.86$) is much higher than at the stream site ($R^2 = 0.31$) because of the smaller range of electrical conductivity than at the landfill. When combining the two data sets, the high coefficient of determination of 0.81 shows it is reasonable to assume a constant formation factor of 4.7 for the two sites. The formation factors determined for the individual measurement points lie between 2.93 and 8.66, which is the formation factor range for unconsolidated sand as reported in the review by Weller et al. (2015). Thus, a formation factor of 4.7 was used at both sites, except for the Postglacial Freshwater Peat layer at the Grindsted stream site where a formation factor of 2.0 was assumed based on the measurements available in the layer.

4.3. Contaminant Mass Discharge Estimation at Grindsted Landfill

4.3.1. Inorganic Conservative Compounds

At the landfill site, the contaminant plume has electrical water conductivity values of up to 430 mS/m, much higher than the background concentration of the studied aquifer, where the electrical water conductivity was between 20 and 30 mS/m. The electrical water conductivity correlates well with the ionic strength,

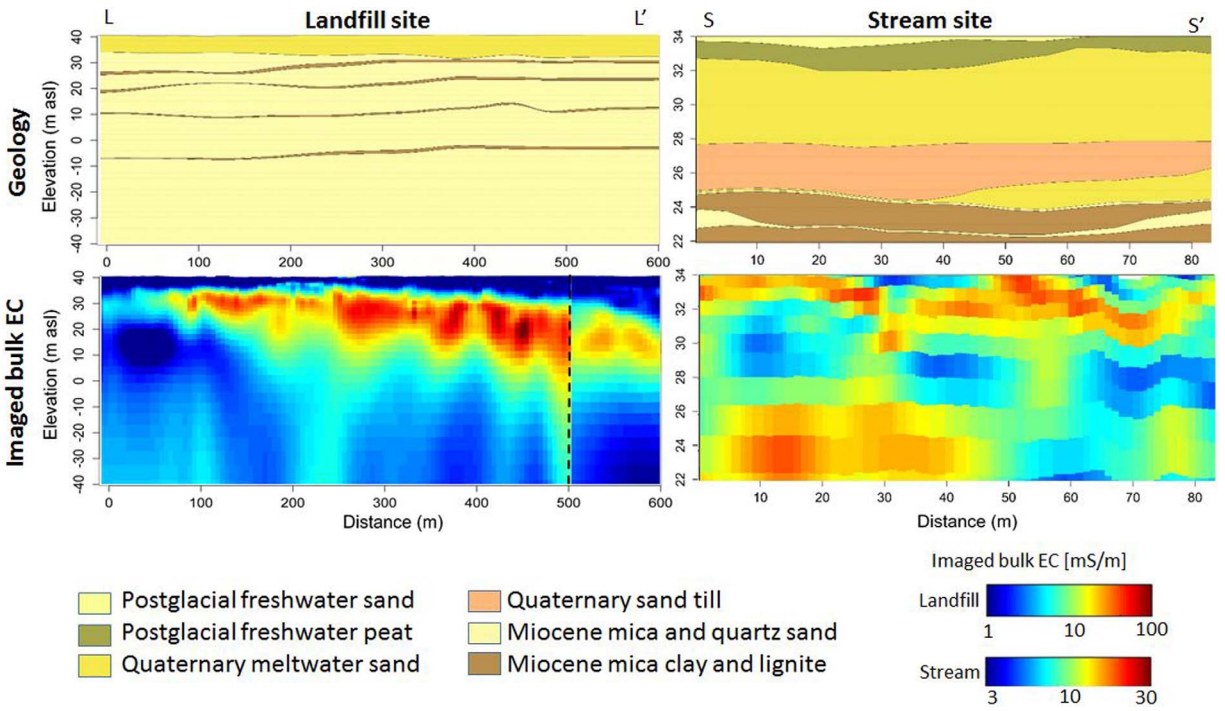

Figure 5. Bulk conductivity and geological model along the LL′ and SS′ control planes at the landfill and stream sites. The distance (*x* axis) is relative to the most southern well of each profile. Note that the landfill and the stream panels have different axes scales. The black dashed line in the landfill panel indicates the point where the two DCIP profiles meet, as shown in Figure 1.

as shown in Figure 7. Thus, the distribution of major cations and anions was investigated. The ions balance depends on the location in the transect; the data shown in Figure 7 describe the core of the contaminant plume (see supporting information Table S5 for all concentration data of major ions available at the landfill). The pie charts show that chloride is the dominant anion and the most important of the inorganic conservative compounds. The multiple regression analysis, performed on the major ions displayed on the pie charts for all water samples (see supporting information Table S6), show that chloride and potassium are the only ions with a statistically significant relationship with the water electrical conductivity. The distribution of concentration of chloride in the plume wells is similar to the distribution of electrical water conductivity, as shown by the coefficient of determination of 0.74. It is important to notice that the point with a very high electrical conductivity value (430 mS/m), in the chloride and ionic strength plot in Figure 7, is a sample collected at the well located at the edge of the hotspot area of the landfill. Thus, higher concentrations of inorganic and organic compounds are expected at that location. The analysis of variance also rejected the null hypothesis of noncorrelation between the water electrical conductivity and chloride (probability values of the *F*-test value are on the order of 10^{-10}, much lower than the selected significance level 0.05). Since chloride is a conservative tracer, these results suggest that electrical water conductivity can be used as an indicator of the location and the migration of the plume in groundwater.

4.3.2. Semipersistent Organic Compounds

Among semipersistent organic compounds, sulfonamides and barbiturates are those found in highest concentration at the landfill site. The range of concentrations of sulfonamides and barbiturates on the control plane is very large, from 0.1 to 67,850 μg/L for sulfonamides and from 0.1 to 5,307 μg/L for barbiturates, so that a logarithmic scale is required in Figure 7. At the site, barbiturates and sulfonamides originate at the same source as chloride and are expected to follow similar transport pathways. Given the similar distributions of the concentration of chloride and electrical water conductivity at the site, the distribution of concentrations of sulfonamides and barbiturates may be similar to the distribution of chloride and, thus, to the electrical water conductivity. The analysis of variance indicated that the null hypothesis of independence of observations between electrical water conductivity and sulfonamides and barbiturates could be rejected (probability values of the *F*-test value are in the order of 10^{-17} and 10^{-15}, respectively, which is much lower than the selected significance level 0.05). Furthermore, high coefficients of determination of 0.82 and 0.77

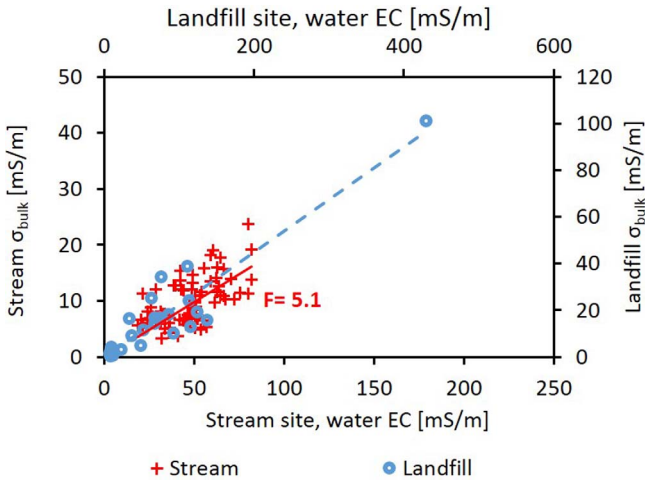

Figure 6. Correlation between the bulk conductivity measured using surface DCIP and the electrical water conductivity from water samples at the landfill and the stream site. Due to different conductivity ranges, values from the stream site are shown on the primary axes and values from the landfill are shown on secondary axes. The solid and dashed lines are trend lines for the stream and the landfill sites, respectively. The formation factor (*F*) calculated as the inverse of the slope of a regression line is indicated on the figure. The selection of samples at the stream site for the correlation plot was based on the following two criteria: (1) the value of the model cells closest to the measured sample points were chosen and (2) sample points only within the DOI and within an horizontal distance up to 1.5 times the electrode spacing from profiles were selected. At the landfill site the same criteria were adopted, but in the second criterion the maximum horizontal distance was 3 times the electrode spacing.

(Figure 7) were obtained for the sulfonamides and barbiturates, respectively. This indicates that, at the site, the electrical water conductivity can be used as an indicator of the concentration distribution of sulfonamides and barbiturates in the plume. Thus, the use of electrical conductivity is promising as a surrogate for the distribution of sulfonamides and barbiturates.

4.3.3. Estimation of the Contaminant Mass Discharge at the Landfill Site

The concentration distributions of chloride, sulfonamides, and barbiturates are shown in Figure 8. The distributions are modeled by the concentration-based and the geophysics-based methods. The distribution of concentrations is used to estimate the contaminant mass discharge, as described in section 3.4. When using the geophysics-based method, the estimated mass discharge is 32,643 kg/yr of chloride, 1,848 kg/yr of sulfonamides, and 112 kg/yr of barbiturates (see supporting information Table S7 for all results). The estimates were lower when using the geophysics-based method compared to the concentration-based method for chloride (by 13%) and higher for sulfonamides (by 146%) and barbiturates (by 27%).

4.4. Contaminant Mass Discharge Estimation at Grindsted Stream

4.4.1. Inorganic and Organic Compounds Affected by Biodegradation

In the plume at the stream site, where the concentrations of ions from the contaminant source are low, depletion of electron acceptors and generation of metabolic by-products (e.g., dissolved iron) associated with the degradation of xenobiotic organic compounds are reflected in the ionic composition in the plume.

When looking at the ion balance (Figure 9) for a water sample collected in the core of the contaminant plume, sodium and dissolved iron are the main cations (the ion balance of all water samples where a full ion analysis was performed is provided in supporting information Table S5). Dissolved iron is generated as a metabolic by-product by biodegradation of organic compounds. The multiple regression analyses performed on all major ions and electrical water conductivity identified dissolved iron as the only ion with a statistically significant relationship with the electrical water conductivity (see supporting information Table S6). A linear correlation between electrical water conductivity and dissolved iron was found (R^2 of 0.78), as shown in Figure 9. Since dissolved iron concentrations are affected by redox processes (see supporting information Table S1), the distribution of dissolved iron (and thus electrical water conductivity) may be similar to the distribution of other compounds affected by redox processes. The distribution of water electrical conductivity is also similar to organic contaminants oxidized during biodegradation (R^2 of 0.67 for benzene and probability value of the *F*-test value of 0.0002, much lower than the selected significance level 0.05).

The high concentrations of dissolved iron, low concentrations of sulfate, and the presence of methane indicate strongly reducing conditions at the control plane. Iron reducing to methanogenic redox conditions facilitate reductive dechlorination, explaining the high concentration of vinyl chloride and *cis*-DCE, compared to PCE and TCE (Rønde et al., 2017). Electrical water conductivity has a similar distribution to that of vinyl chloride (R^2 of 0.93) and *cis*-DCE (R^2 of 0.5). The analysis of variance indicates that the null hypothesis of independence of observations between electrical water conductivity and *cis*-DCE and vinyl chloride could be rejected (probability values of the *F*-test value are in the order of 0.001 and 10^{-9}, respectively, much lower than the selected significance level 0.05).

4.4.2. Contaminant Mass Discharge Estimation at the Stream Site

At the stream site (Figure 10), the highest concentrations of benzene, *cis*-DCE, and vinyl chloride are found in the Quaternary sand layer, above the sand till. This distribution is reflected in the kriged planes. On the left most 10 m sections of the profile, relatively high concentrations are found below 28 m asl. A similar result is shown by the kriged concentration profile where for vinyl chloride, concentrations higher than

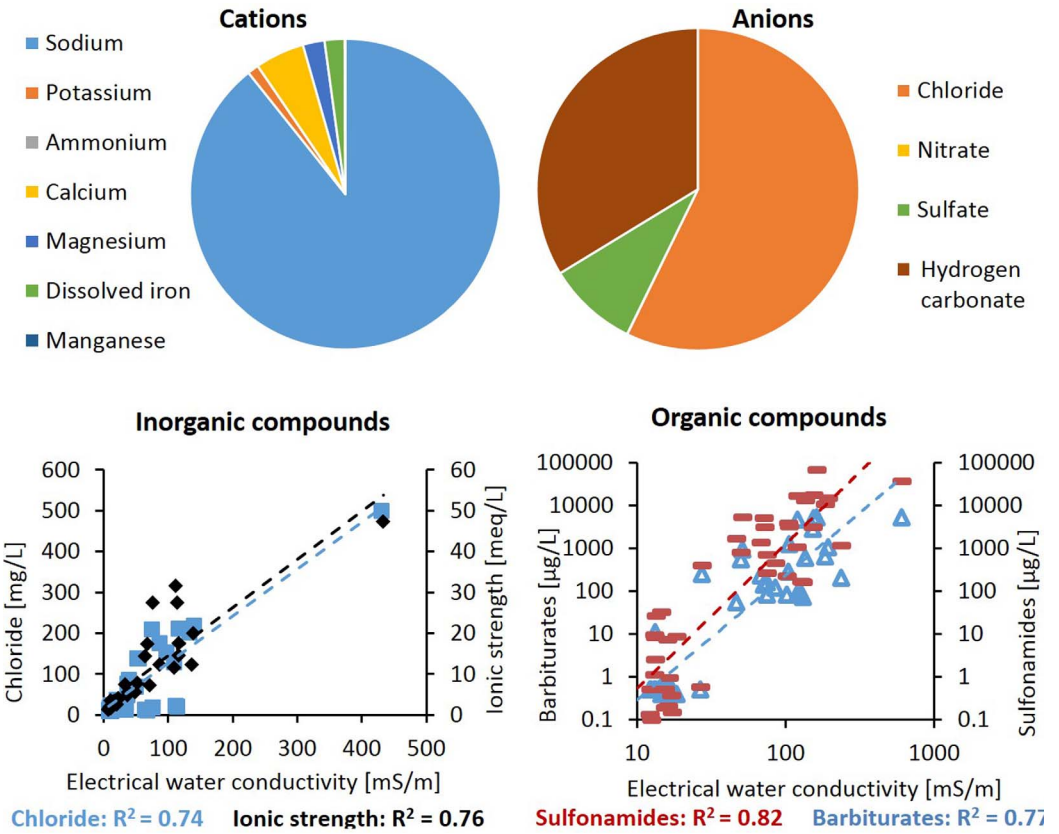

Figure 7. The pie charts show the distribution of cations and anions in eq/L at a screen located in the middle of the contaminant plume at the landfill site (see supporting information Table S5 for data and location of the well). The cross plots show the concentration electrical water conductivity and selected organic and inorganic compounds present in the contaminant plume at the landfill site. Note that the regression of the electrical water conductivity and xenobiotic organic compounds at the landfill are power law regressions, and are shown with a log-log plot. The other regressions are linear.

0.1 mg/L, are predicted below the sand till layer (25 m asl). This may indicate that the plume is not fully covered by the boreholes in the control plane in this area.

The estimated mass discharges are 48 and 49 kg/L of vinyl chloride, 51 and 52 kg/L of cis-DCE, and 12 and 11 kg/L of benzene, when using the concentration-based and geophysics-based method, respectively (see supporting information Table S7 for all results). In contrast to the landfill site, where a considerable difference was found in the contaminant mass discharge estimated by the two methods, the estimated contaminant mass discharges using the two methods agreed well at the stream site for all three compounds. This can be explained by the much higher sample density at the stream site (0.06 samples/m^2) compared to that at the landfill (0.0004 samples/m^2).

4.5. Error Analyses for the Contaminant Mass Discharge

The average contaminant mass discharge error (calculated from equation (9)) and relative uncertainty (calculated from equation (10)) are shown in Figure 11 as a function of the sample density. The error and uncertainty analysis are shown for chloride from the landfill site and for vinyl chloride from the stream site. In Table 1, the average contaminant mass discharge values used to calculate the average relative error are shown for all tested sample densities and corresponding number of samples. The analysis was also performed for barbiturates at the landfill site, showing similar results to chloride. Thus, only the results for chloride are presented here (see supporting information Table S7–S8 for the results for barbiturates).

The contaminant mass discharge relative error is inversely proportional to the number of samples for both tested compounds. The geophysics-based method has an error consistently lower than the contaminant concentrations method. The error difference between the two methods increases with the sample density.

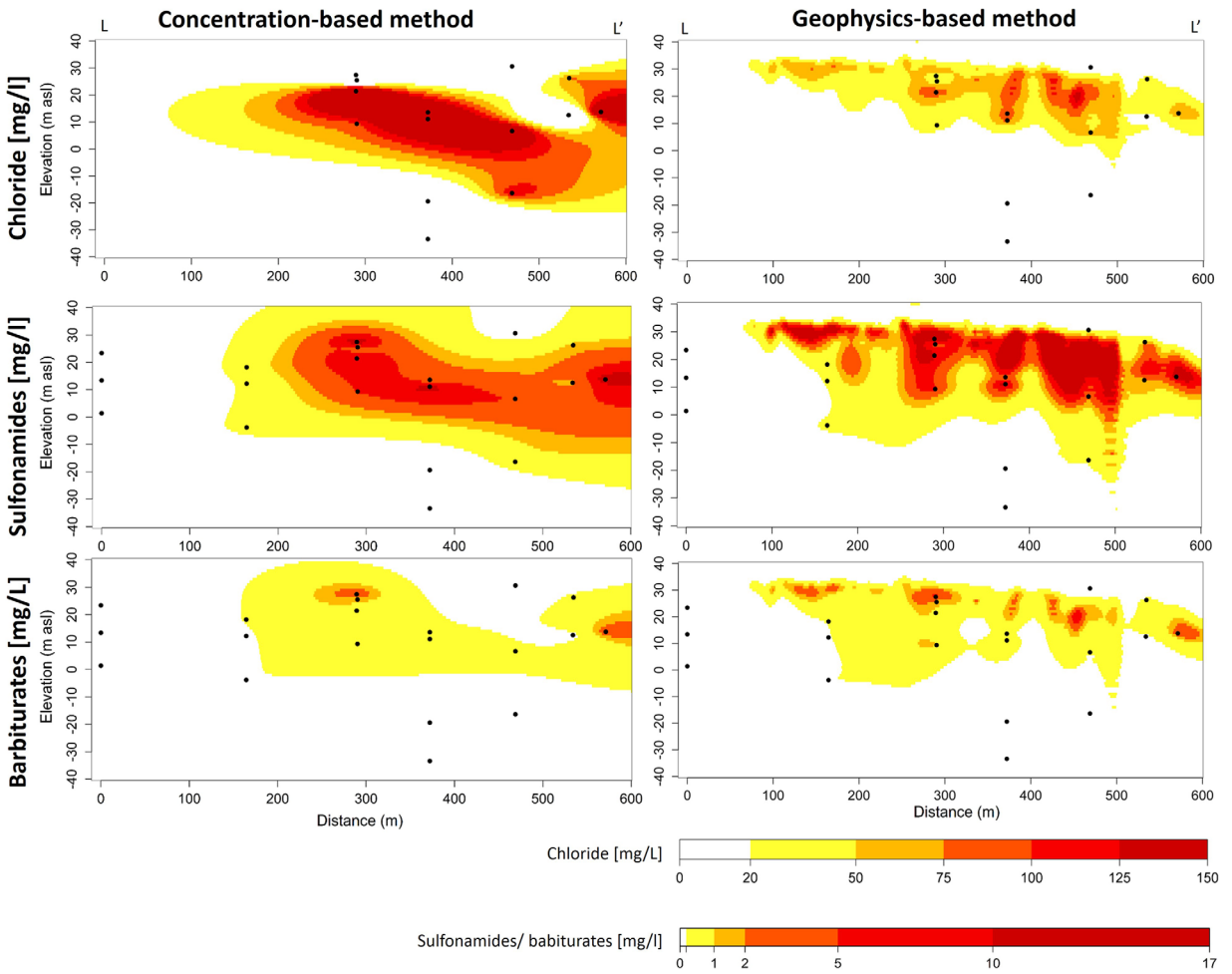

Figure 8. Contaminant concentration distribution modeled by the concentration-based and by the geophysics-based approach along the control plane at the Grindsted landfill site of chloride, sulfonamides, and barbiturates. The black dots show the location of water samples.

At the lowest tested sample density (0.0001 samples/m^2) at the landfill site, the error of the geophysics-based method is 10 times lower compared to the concentration-based method.

The relative uncertainty of the contaminant mass discharge is also inversely proportional to the sample density. The uncertainties of the two methods are very similar at the Grindsted stream site for vinyl chloride. At the Grindsted landfill site, the uncertainty of the geophysics-based method is 4 times lower than the uncertainty of the concentration-based method. Differences in the uncertainty and error analysis between the two sites can be related to the much lower sample density at the landfill site, compared to the stream site.

5. Discussion

In the following section, the geophysics-based method is discussed in order to identify the advantages and the limitations of its applicability when compared to the concentration-based method.

The relative error is inversely proportional to the sample density both for the concentration-based method and the geophysics-based method. This result is in accordance with previous studies (e.g., Kübert & Finkel, 2006; Troldborg et al., 2012). The difference between the errors calculated by the two methods increases with the sample density, suggesting that the geophysics-based approach is less dependent on the number of water samples and their location than the concentration-based approach. However, the difference is modest with high sampling densities indicating that the method is most beneficial at sites with low sampling densities.

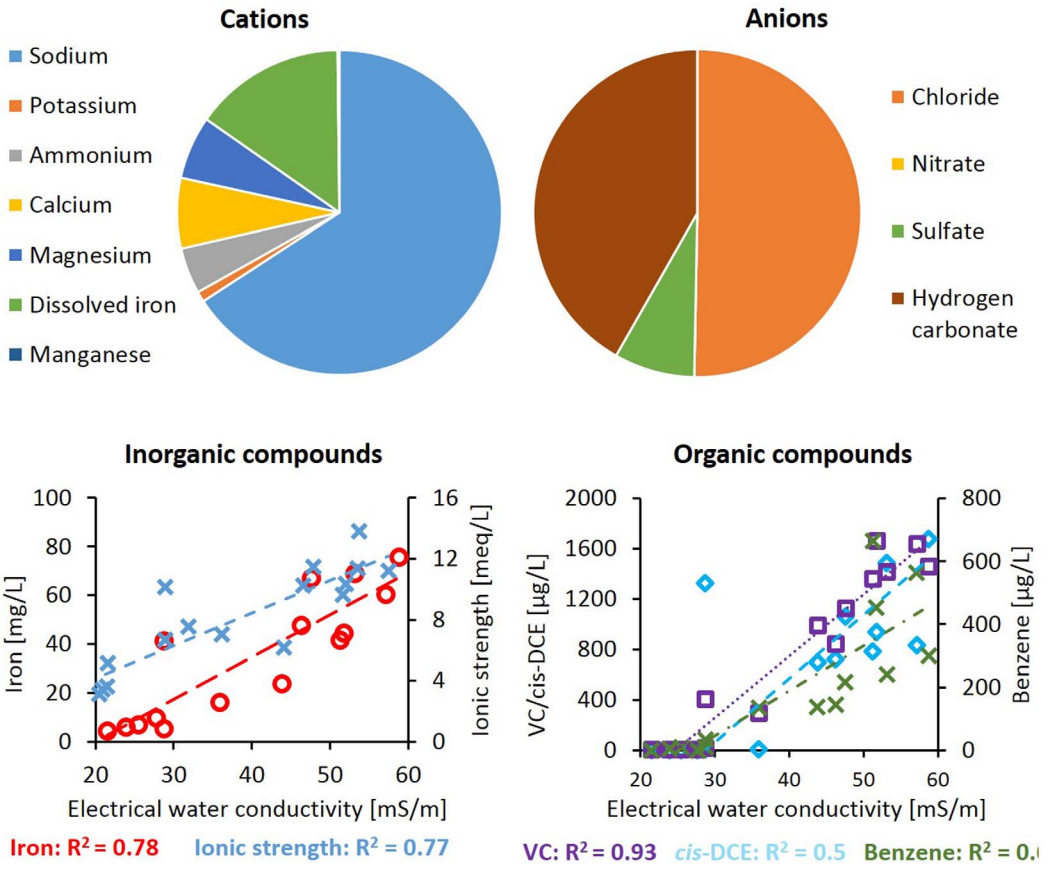

Figure 9. The pie charts show the distribution of cations and anions in eq/L at a screen located in the middle of the contaminant plume few meters upstream of the investigated transect at the stream site (see supporting information Table S5 for data and location of the well). The cross plots show the concentration of electrical water conductivity and selected organic and inorganic compounds present in the contaminant plume at the stream site. All regressions are linear. Please note that the *x* axis starts at 20 mS/m.

The geophysics-based approach relies on being able to correlate the imaged bulk conductivity from DCIP to the water chemistry, through the electrical water conductivity. The electrical water conductivity is dependent on the concentration of total ions in the water. Depending on characteristics of the source and the biogeochemical processes taking place in the aquifer, the distribution of total ions (thus electrical water conductivity) may be similar to the distribution of specific ions or xenobiotic organic compounds. The sites presented in this study have plumes with different water chemistry. At the landfill site, the leachate plume has high concentrations of ions released from the landfill. Here the distribution of electrical water conductivity in the plume was similar to the distribution of a conservative ionic species (chloride) and semipersistent organic species (sulfonamides and barbiturates). The plume at the stream site has a much lower concentration of ions; thus, changes in the redox species due to microbial biodegradation have stronger impact on electrical water conductivity. As described in the review by Atekwana and Slater (2009), microbial activity can play a key role in redox processes and greatly affect the fluid chemistry, as seen in the geophysical signature (e.g., Aal et al., 2004; Allen et al., 2007; Atekwana & Atekwana, 2010). In our study, it was possible to find a linear link between bulk and electrical water conductivity and the redox-sensitive parameters, such as dissolved iron. Masi and Losito (2015) highlighted the importance of pH dependent processes on the DCIP surveys. Along the investigated transects, the pH mainly falls between 5 and 7; thus, the electrical conductivity is not highly affected by changes in the pH.

Previous studies have measured DC resistivity and IP anomalies at contaminant plumes caused by physical changes on the grain surface due to biofilm formation during microbial biodegradation and iron precipitates (Aal et al., 2004; Atekwana & Atekwana, 2010; Atekwana & Slater, 2009; Personna et al., 2013; Williams

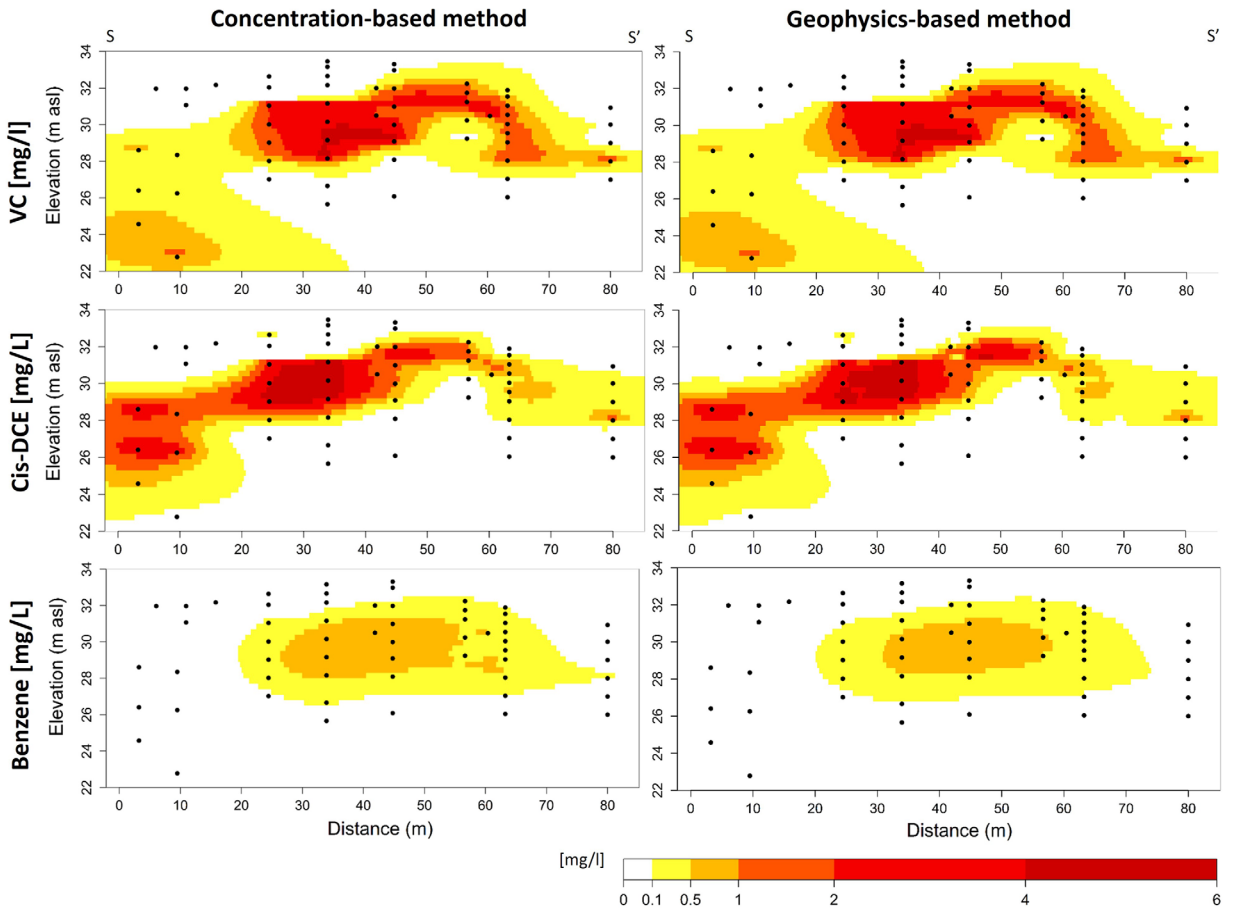

Figure 10. Contaminant concentration distribution modeled by the concentration-based and by the geophysics-based approach along the control plane at the Grindsted stream site of vinyl chloride, *cis*-DCE, and benzene. The black dots show the location of water samples.

et al., 2009). In our study, we use the IP data to remove the effect of surface conductivity from the bulk conductivity, and this is possible under the assumption that the IP signal is controlled by the surface area of the sediments, and not by the presence of, e.g., biofilms and/or iron precipitates. Iron precipitates (e.g., siderite)

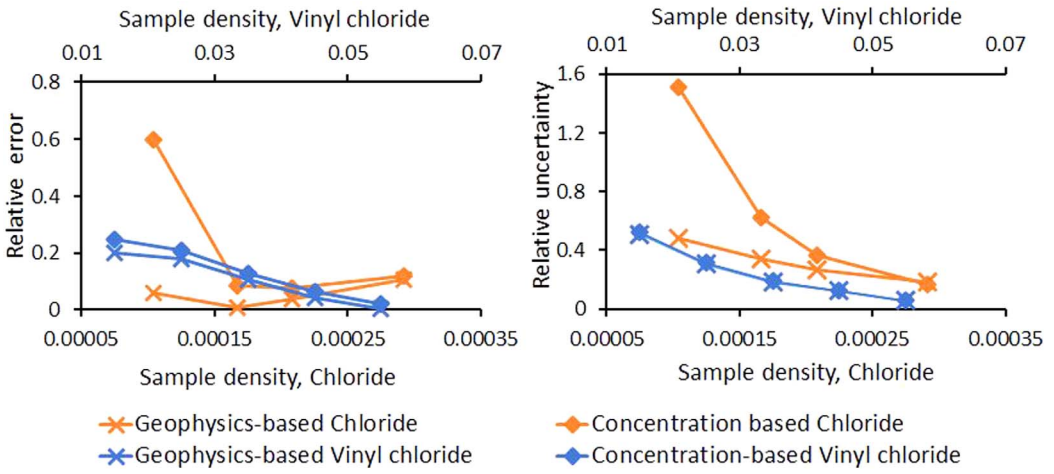

Figure 11. Relative error and uncertainty of the geophysics-based and concentration-based methods for estimating the mass discharge of barbiturates as a function of the sample density. The analysis is performed for chloride at the Grindsted landfill site and for vinyl chloride at the Grindsted stream site. Notice the two different *x* axes due to the different number of samples available at the site.

Table 1
Average Contaminant Mass Discharge at Different Sampling Densities for Chloride and Vinyl Chloride at the Grindsted Landfill and Stream Site, Respectively

		Sample density (n of samples/m^2)	Number of samples	Method	Contaminant mass discharge (kg/yr)
Landfill site	All data	0.0003	14	Conc	37,374
	Subset of data	0.00025	12	Conc	32,943
				Geophys	33,421
		0.00020	10	Conc	34,476
				Geophys	35,916
		0.00015	8	Conc	34,230
				Geophys	37,762
		0.00010	5	Conc	59,740
				Geophys	39,647
Stream site	All data	0.060	58	Conc	48
	Subset of data	0.055	53	Conc	47
				Geophys	48
		0.045	43	Conc	45
				Geophys	46
		0.035	34	Conc	42
				Geophys	43
		0.025	24	Conc	38
				Geophys	39
		0.015	14	Conc	36
				Geophys	38

Note. The contaminant mass discharge values are calculated from 1,000 stochastic simulations for sample densities. Results are shown for the geophysics-based approach (Geophys) and concentration-based approached (Conc).

have been identified in the upper part of the landfill leachate plume (Heron et al., 1998). Since the concentrations are low and most pronounced in the Quaternary sediments, this is not expected to be a controlling factor, especially in the deeper Miocene parts of the aquifer with high contaminant concentrations. The microbial numbers are very small at the site (Ludvigsen et al., 1998), so the presence a biofilm at the site is very unlikely. Indeed, the variability in the IP parameters at the site is explained well by the local lithology and by the changes in the bulk conductivity values.

As described in section 3.5, it is important to understand the reasons behind the conceptual link between water electrical conductivity and the semipersistent xenobiotic organic compounds and biodegradable xenobiotic organic compounds. Semipersistent xenobiotic organic compounds, such as pharmaceutical compounds, can be correlated with electrical water conductivity when an inorganic plume originates from the same source and has a similar travel path as the organic plume. This was the case at the Grindsted landfill site, but at other sites the distribution of inorganic and organic compounds in the contaminant source may be different. The link between the electrical water conductivity and benzene, a biodegradable xenobiotic organic compound was found in this study at the Grindsted stream site. Such a link can be found if xenobiotic organic compound degradation is substantial and the production of reduced iron affects the overall distribution of ions. However, a link between degradable xenobiotic organic compounds and electrical water conductivity may be difficult to establish at sites where plumes also have large inorganic ion concentrations or where the main redox driver is organic carbon, such as landfill sites like the Grindsted landfill (Bjerg et al., 1995; Christensen et al., 2001). Chlorinated ethenes are also biodegradable and their distribution often depends on redox conditions (Badin et al., 2016; Chambon et al., 2013). Electrical water conductivity can be linked to *cis*-DCE or vinyl chloride concentrations, through the relationship with ionic redox byproducts (e.g., dissolved iron), such as at the Grindsted stream site.

The geophysics-based approach relies on the imaging of bulk conductivity from DCIP data. The resolution of the surface DCIP method decreases with depth and the inversion models are not reliable below the depth of investigation. In this study, the investigated transects were inside the depth of investigation (see Figure 4 and Maurya et al. (2018) for the Grindsted stream site and Maurya et al. (2017) for the Grindsted landfill site). Furthermore, the disentanglement of the bulk conductivity and the surface conductivity relies on the effectiveness of equation (3) (Weller et al., 2013).

The concentration field obtained by combining DCIP and water-sample data was found using regression kriging. Regression kriging has been previously used to combine geophysical and hydrological data. De Benedetto et al. (2012) used the same method for modeling the spatial distribution of clay content in soil and De Benedetto et al. (2013) applied the method for estimating the soil moisture content. Estimates of contaminant mass discharge based on kriging can be very uncertain, especially when few water-sample data are available. Regression kriging, used to combine geophysical information and contaminant concentrations, requires contaminant concentration data to derive a variogram model of residuals. Similarly, the ordinary kriging employed to interpolate contaminant concentration data also requires a variogram model of the concentration. When the number of samples is very low, the fitted variogram model deteriorates or cannot be derived, resulting in a poor estimation. At the stream site, the analysis of the relative uncertainty showed an uncertainty of 51% and 52% at the lowest analyzed sample density (0.015 samples/m^2), depending on the method. These uncertainties are similar to the uncertainty ($\sim$60%) calculated by Troldborg et al. (2012) for a sample density of 0.02 samples/m^2.

The uncertainty analysis performed in this study does not account for geological heterogeneity, but such heterogeneity is important when estimating contaminant mass discharge (Troldborg et al., 2010). The assumption of a constant groundwater flow velocity affects both the contaminant discharge estimation and its uncertainty. The impact of geologic heterogeneity has not been investigated in this study because the focus has been on using surface DCIP to describe the spatial distribution of bulk conductivity and hence of organic contaminants. Furthermore, the two field sites analyzed in this study were only mildly heterogeneous. For instance, at the landfill site, the variance of the ln K is 0.7, while the variances of the log-normalized concentrations of barbiturates and sulfonamides are 11 and 18. Thus, the changes in the groundwater flow field at the site will have a lower impact on the contaminant mass discharge than the distribution of contaminant concentrations. The recent works of Weller et al. (2015), Fiandaca et al. (2018b), and Maurya et al. (2018), suggest that induced polarization data can reproduce the spatial distribution of hydraulic conductivities. Therefore, it may be possible to generalize the results of this study to more heterogeneous settings.

Finally, the method presented here is particularly promising at sites where high sampling densities are infeasible such as deep aquifers (because of high drilling cost) or large contaminated sites such as abandoned landfills and former industrial production facilities. For practical purposes, DCIP surveys should be incorporated into site investigations at an early stage. DCIP can guide the placement of boreholes and can be combined with geological modeling to calculate the contaminant mass discharge with the new method proposed in this paper.

6. Conclusions

The geophysics-based method for contaminant mass discharge presented in this paper is designed to improve the interpolation of contaminant concentration data at large contaminated sites, where the number of water-sample points is often limited compared to the size of the control plane.

The method relies on finding a conceptual link between the bulk conductivity imaged using the DCIP and the concentration of contaminants. The method was successful estimating the contaminant mass discharge of chloride and pharmaceutical compounds (sulfonamides and barbiturates) at a landfill site. At a contaminant plume from a former pharmaceutical industry, the method was applied for benzene and chlorinated ethenes (vinyl chloride and *cis*-DCE). However, the conceptual links are site specific and depend on the chemical composition of the contaminant plume and on the solute transport processes. Thus, the method is suitable for contaminant plumes characterized by high concentration of ionic species released from the source, such as landfill leachate plume. The method can also be applied at sites where the redox processes and their ionic by-products can affect the ion balance of the inorganic compounds.

The estimation error of the integrated method was compared to the traditional method of kriging water-sample data by stochastically simulating data sets with different sample densities. Results showed that the relative error increases when decreasing the sampling density. The geophysics-based method was shown to be more accurate than the traditional method using only contaminant concentrations, with the tested sample densities (0.055–0.015 samples/m^2). The difference between the two methods is negatively correlated with the sampling density. At the lower tested sample density, the geophysics-based method

estimates the contaminant mass discharge to have a relative error that is 24% lower than the concentration-based method. This indicates that the geophysical-based method is less dependent on the number of water samples and their location. Thus, the method is ideal for large contaminated sites and/or deep plumes where the number of water samples is often low for describing the extension of the contaminant plume and estimating the contaminant mass discharge.

Acknowledgments
This study was supported by the research project GEOCON, Advancing GEOlogical, geophysical and CONtaminant monitoring technologies for contaminated site investigation (contract 1305-00004B). The funding for GEOCON is provided by Innovation Fund Denmark. Particular thanks to our colleagues at DTU environment, Bent H. Skov, Jens S. Sørensen, Flemming Møller, and Erik R. Lange for assistance in the field; Hanne Bøggild, Sinh Hy Nguyen, and Satomi Matsuura for carrying out the chemical analyses. Thanks to Wolfgang Nowak for useful discussions on the calculation of mass discharge. Thanks to Associate Editor, Lee Slater, Research Hydrologist, PhD, Isabelle M. Cozzarelli, and two anonymous reviewers for their helpful comments. Hydrogeological data are provided by Maurya et al. (2018) and Rønde et al. (2017) for the Grindsted stream. Geophysical data are provided by Maurya et al. (2018) for Grindsted stream site and Maurya et al. (2017) for the Grindsted landfill site. Chemical data are provided in the supporting information (supporting information Tables S2–S5).

References

Aal, G. Z. A., Atekwana, E. A., Slater, L. D., & Atekwana, E. A. (2004). Effects of microbial processes on electrolytic and interfacial electrical properties of unconsolidated sediments. *Geophysical Research Letters*, *31*, L12505. https://doi.org/10.1029/2004GL020030

Allen, J. P., Atekwana, E. A., Atekwana, E. A., Duris, J. W., Werkema, D. D., & Rossbach, S. (2007). The microbial community structure in petroleum-contaminated sediments corresponds to geophysical signatures. *Applied and Environmental Microbiology*, *73*(9), 2860–2870. https://doi.org/10.1128/AEM.01752-06

Appelo, C. A. J., & Postma, D. (2005). *Geochemistry, groundwater and pollution* (2nd ed.). Amsterdam, the Netherlands: CRC Press.

Archie, G. E. (1942). The electrical resistivity log as an aid in determining some reservoir characteristics. *Transactions of the American Institute of Mining and Metallurgical Engineers*, *146*, 54–62.

Atekwana, E. A., & Atekwana, E. A. (2010). Geophysical signatures of microbial activity at hydrocarbon contaminated sites: A review. *Surveys in Geophysics*, *31*(2), 247–283. https://doi.org/10.1007/s10712-009-9089-8

Atekwana, E. A., & Slater, L. D. (2009). Biogeophysics: A new frontier in earth science research. *Reviews of Geophysics*, *47*, RG4004. https://doi.org/10.1029/2009RG000285

Badin, A., Broholm, M. M., Jacobsen, C. S., Palau, J., Dennis, P., & Hunkeler, D. (2016). Identification of abiotic and biotic reductive dechlorination in a chlorinated ethene plume after thermal source remediation by means of isotopic and molecular biology tools. *Journal of Contaminant Hydrology*, *192*, 1–19. https://doi.org/10.1016/j.jconhyd.2016.05.003

Balbarini, N., Boon, W. M., Nicolajsen, E., Nordbotten, J. M., Bjerg, P. L., & Binning, P. J. (2017). A 3-D numerical model of the influence of meanders on groundwater discharge to a gaining stream in an unconfined sandy aquifer. *Journal of Hydrology*, *552*, 168–181. https://doi.org/10.1016/j.jhydrol.2017.06.042

Binley, A. (2015). Tools and techniques: DC electrical methods. In G. Schubert (Ed.), *Treatise on geophysics* (2nd ed., Vol. 11, pp. 233–259). Amsterdam, the Netherlands: Elsevier. https://doi.org/10.1016/B978-0-444-53802-4.00192-5

Bjerg, P. L., Rügge, K., Pedersen, J. K., & Christensen, T. H. (1995). Distribution of redox-sensitive groundwater quality parameters downgradient of a landfill (Grindsted, Denmark). *Environmental Science and Technology (Washington)*, *29*(5), 1387–1394. https://doi.org/10.1021/es00005a035

Bjerg, P. L., Tuxen, N., Reitzel, L., Albrechtsen, H.-J., & Kjeldsen, P. (2011). Natural attenuation processes in landfill leachate plumes at three Danish sites. *Ground Water*, *49*(5), 688–705. https://doi.org/10.1111/j.1745-6584.2009.00613.x

Bockelmann, A., Zamfirescu, D., Ptak, T., Grathwohl, P., & Teutsch, G. (2003). Quantification of mass fluxes and natural attenuation rates at an industrial site with a limited monitoring network: A case study. *Journal of Contaminant Hydrology*, *60*(1–2), 97–121. https://doi.org/10.1016/S0169-7722(02)00060-8

Bohling, G. C., Liu, G., Knobbe, S. J., Reboulet, E. C., Hyndman, D. W., Dietrich, P., et al. (2012). Geostatistical analysis of centimeter-scale hydraulic conductivity variations at the MADE site. *Water Resources Research*, *48*, W02525. https://doi.org/10.1029/2011WR010791

Cai, Z., Wilson, R. D., Cardiff, M. A., & Kitanidis, P. K. (2011). Increasing confidence in mass discharge estimates using geostatistical methods. *Ground Water*, *49*(2), 197–208. https://doi.org/10.1111/j.1745-6584.2010.00709.x

Chambers, J. E., Kuras, O., Meldrum, P. I., Ogilvy, R. D., & Hollands, J. (2006). Electrical resistivity tomography applied to geologic, hydrogeologic, and engineering investigations at a former waste-disposal site. *Geophysics*, *71*(6), B231–B239. https://doi.org/10.1190/1.2360184

Chambon, J. C. C., Bjerg, P. L., Scheutz, C., Bælum, J., Jakobsen, R., & Binning, P. J. (2013). Review of reactive kinetic models describing reductive dechlorination of chlorinated ethenes in soil and groundwater. *Biotechnology and Bioengineering*, *110*(1), 1–23. https://doi.org/10.1002/bit.24714

Christensen, T. H., Bjerg, P. L., Banwarth, S. A., Jakobsen, R., Heron, G., & Albrechtsen, H.-J. (2000). Characterization of redox conditions in groundwater contaminant plumes. *Journal of Contaminant Hydrology*, *45*(3–4), 165–241. https://doi.org/10.1016/S0169-7722(00)00109-1

Christensen, T. H., Kjeldsen, P., Bjerg, P. L., Jensen, D. L., Christensen, J. B., Baun, A., et al. (2001). Biogeochemistry of landfill leachate plumes. *Applied Geochemistry*, *16*(7–8), 659–718. https://doi.org/10.1016/S0883-2927(00)00082-2

Cozzarelli, I. M., Boehlke, J. K., Masoner, J., Breit, G. N., Lorah, M. M., Tuttle, M. L. W., et al. (2011). Biogeochemical evolution of a landfill leachate plume, Norman, Oklahoma. *Ground Water*, *49*(5), 663–687. https://doi.org/10.1111/j.1745-6584.2010.00792.x

Dahlin, T., Rosqvist, H., & Leroux, V. (2010). Resistivity-IP mapping for landfill applications. *First Break*, *28*(8).

Dahlin, T., & Zhou, B. (2006). Multiple-gradient array measurements for multichannel 2D resistivity imaging. *Near Surface Geophysics*, *4*(2), 113–123.

De Benedetto, D., Castrignano, A., & Quarto, R. (2013). A geostatistical approach to estimate soil moisture as a function of geophysical data and soil attributes. *Procedia Environmental Sciences*, *19*, 436–445. https://doi.org/10.1016/j.proenv.2013.06.050

De Benedetto, D., Castrignano, A., Sollitto, D., Modugno, F., Buttafuoco, G., & lo Papa, G. (2012). Integrating geophysical and geostatistical techniques to map the spatial variation of clay. *Geoderma*, *171*(Sp. Iss. SI), 53–63. https://doi.org/10.1016/j.geoderma.2011.05.005

Fiandaca, G., Auken, E., Christiansen, A. V., & Gazoty, A. (2012). Time-domain-induced polarization: Full-decay forward modeling and 1D laterally constrained inversion of Cole–Cole parameters. *Geophysics*, *77*(3), E213–E225. https://doi.org/10.1190/geo2011-0217.1

Fiandaca, G., Christiansen, A. V., & Auken, E. (2015). Depth of investigation for multi-parameters inversions. In *21st European Meeting of Environmental and Engineering Geophysics* (pp. 666–670). https://doi.org/10.3997/2214-4609.201413797

Fiandaca, G., Maurya, P. K., Balbarini, N., Hördt, A., Christiansen, A. V., Foged, N., et al. (2018b). Permeability estimation directly from logging-while-drilling Induced Polarization data. *Water Resources Research*, *54*. https://doi.org/10.1002/2017WR022411, in press.

Fiandaca, G., Meldgaard Madsen, L., & Maurya, P. K. (2018a). Re-parameterizations of the Cole–Cole model for improved spectral inversion of induced polarization data. *Near Surface Geophysics*. https://doi.org/10.3997/1873-0604.2017065.

Fiandaca, G., Ramm, J., Binley, A., Gazoty, A., Christiansen, A. V., & Auken, E. (2013). Resolving spectral information from time domain induced polarization data through 2-D inversion. *Geophysical Journal International*, *192*(2), 631–646. https://doi.org/10.1093/gji/ggs060

Frid, V., Sharabi, I., Frid, M., & Averbakh, A. (2017). Leachate detection via statistical analysis of electrical resistivity and induced polarization data at a waste disposal site (Northern Israel). *Environmental Earth Sciences*, *76*(6), 233. https://doi.org/10.1007/s12665-017-6554-4

Gazoty, A., Fiandaca, G., Pedersen, J., Auken, E., & Christiansen, A. V. (2012a). Mapping of landfills using time-domain spectral induced polarization data: The Eskelund case study. *Near Surface Geophysics*, *10*(6), 575–586. https://doi.org/10.3997/1873-0604.2012046

Gazoty, A., Fiandaca, G., Pedersen, J., Auken, E., Christiansen, A. V., & Pedersen, J. K. (2012b). Application of time domain induced polarization to the mapping of lithotypes in a landfill site. *Hydrology and Earth System Sciences*, *16*(6), 1793–1804. https://doi.org/10.5194/hess-16-1793-2012

Guilbeault, M. A., Parker, B. L., & Cherry, J. A. (2005). Mass and flux distributions from DNAPL zones in sandy aquifers. *Ground Water*, *43*(1), 70–86. https://doi.org/10.1111/j.1745-6584.2005.tb02287.x

Hengl, T. (2009). *A practical guide to geostatistical mapping, EUR 22904 EN scientific and technical research series*. Office for Official Publications of the European Communities.

Hengl, T., Heuvelink, G. B. M., & Rossiter, D. G. (2007). About regression-kriging: From equations to case studies. *Computers and Geosciences*, *33*(10), 1301–1315. https://doi.org/10.1016/j.cageo.2007.05.001

Heron, G., Bjerg, P. L., Gravesen, P., Ludvigsen, L., & Christensen, T. H. (1998). Geology and sediment geochemistry of a landfill leachate contaminated aquifer (Grindsted, Denmark). *Journal of Contaminant Hydrology*, *29*(4), 301–317.

Holm, J. V., Rügge, K., Bjerg, P. L., & Christensen, T. H. (1995). Occurrence and distribution of pharmaceutical organic compounds in the groundwater downgradient of a landfill (Grindsted, Denmark). *Environmental Science & Technology*, *29*(5), 1415–1420.

Johansen, H. K., & Sørensen, K. (1979). Fast hankel transforms. *Geophysical Prospecting*, *27*(4), 876–901.

Johansson, S., Sparrenbom, C., Fiandaca, G., Lindskog, A., Olsson, P. I., Dahlin, T., et al. (2016). Investigations of a Cretaceous limestone with spectral induced polarization and scanning electron microscopy. *Geophysical Journal International*, *208*(2), 954–972.

Kemna, A., Binley, A., & Slater, L. (2004). Crosshole IP imaging for engineering and environmental applications. *Geophysics*, *69*(1), 97–107.

Kjeldsen, P., Bjerg, P. L., Rügge, K., Christensen, T. H., & Pedersen, J. K. (1998a). Characterization of an old municipal landfill (Grindsted, Denmark) as a groundwater pollution source: Landfill hydrology and leachate migration. *Waste Management and Research*, *16*(1), 14–22.

Kjeldsen, P., Grundtvig, A., Winther, P., & Andersen, J. S. (1998b). Characterization of an old municipal landfill (Grindsted, Denmark) as a groundwater pollution source: Landfill history and leachate composition. *Waste Management and Research*, *16*(1), 3–13.

Kübert, M., & Finkel, M. (2006). Contaminant mass discharge estimation in groundwater based on multi-level point measurements: A numerical evaluation of expected errors. *Journal of Contaminant Hydrology*, *84*(1–2), 55–80. https://doi.org/10.1016/j.jconhyd.2005.12.003

Lesmes, D. P., & Frye, K. M. (2001). Influence of pore fluid chemistry on the complex conductivity and induced polarization responses of Berea sandstone. *Journal of Geophysical Research*, *106*(B3), 4079–4090. https://doi.org/10.1029/2000JB900392

Li, K. B., & Abriola, L. M. (2009). A multistage multicriteria spatial sampling strategy for estimating contaminant mass discharge and its uncertainty. *Water Resources Research*, *45*, W06407. https://doi.org/10.1029/2008WR007362

Ludvigsen, L., Albrechtsen, H.-J., Heron, G., Bjerg, P. L., & Christensen, T. H. (1998). Anaerobic microbial redox processes in a landfill leachate contaminated aquifer (Grindsted, Denmark). *Journal of Contaminant Hydrology*, *33*, 273–291.

Mackay, D. M., Einarson, M. D., Kaiser, P. M., Nozawa-Inoue, M., Goyal, S., Chakraborty, I., et al. (2012). Mass discharge in a tracer plume: Evaluation of the Theissen Polygon Method. *Ground Water*, *50*(6), 895–907. https://doi.org/10.1111/j.1745-6584.2012.00912.x

Masi, M., & Losito, G. (2015). Spectral induced polarization for monitoring electrokinetic remediation processes. *Journal of Applied Geophysics*, *123*, 284–294. https://doi.org/10.1016/j.jappgeo.2015.08.011

Matheron, G. (1973). The intrinsic random functions and their applications. *Advances in Applied Probability*, *5*(3), 439–468. https://doi.org/10.2307/1425829

Maurya, P. K., Balbarini, N., Møller, I., Rønde, V., Christiansen, A. V., Bjerg, P. L., et al. (2018). Subsurface imaging of water electrical conductivity, hydraulic permeability and lithology at contaminated sites by induced polarization. *Geophysical Journal International*, *213*(2), 770–785. https://doi.org/10.1093/gji/ggy018

Maurya, P. K., Rønde, V., Fiandaca, G., Balbarini, N., Auken, E., Bjerg, P. L., et al. (2017). Detailed landfill leachate plume mapping using 2D and 3D Electrical Resistivity Tomography—With correlation to ionic strength measured in screens. *Journal of Applied Geophysics*, *138*, 1–8. https://doi.org/10.1016/j.jappgeo.2017.01.019

McBratney, A. B., Santos, M. L. M., & Minasny, B. (2003). On digital soil mapping. *Geoderma*, *117*(1–2), 3–52. https://doi.org/10.1016/S0016-7061(03)00223-4

Odeh, I. O. A., McBratney, A. B., & Chittleborough, D. J. (1995). Further results on prediction of soil properties from terrain attributes—Heterotopic cokriging and regression-kriging. *Geoderma*, *67*(3–4), 215–226. https://doi.org/10.1016/0016-7061(95)00007-B

Ogilvy, R., Meldrum, P., Chambers, J., & Williams, G. (2002). The use of 3D electrical resistivity tomography to characterise waste and leachate distribution within a closed landfill, Thriplow, UK. *Journal of Environmental and Engineering Geophysics*, *7*(1), 11–18. https://doi.org/10.4133/JEEG7.1.11

Olsson, P.-I., Fiandaca, G., Larsen, J. J., Dahlin, T., & Auken, E. (2016). Doubling the spectrum of time-domain induced polarization by harmonic de-noising, drift correction, spike removal, tapered gating and data uncertainty estimation. *Geophysical Journal International*, *207*(2), 774–784. https://doi.org/10.1093/gji/ggw260

Pedersen, M. L., Sode, A., Kaarup, P., & Bundgaard, P. (2006). *Habitat quality in Danish streams. Testing of two indices and development of a national physical habitat quality index* (Sci. Rep. 590) [in Danish]. Silkeborg, Denmark: National Environmental Research Institute.

Pelton, W. H., Ward, S. H., Hallof, P. G., Sill, W. R., & Nelson, P. H. (1978). Mineral discrimination and removal of inductive coupling with multifrequency IP. *Geophysics*, *43*(3), 588–609.

Personna, Y. R., Slater, L., Ntarlagiannis, D., Werkema, D., & Szabo, Z. (2013). Complex resistivity signatures of ethanol biodegradation in porous media. *Journal of Contaminant Hydrology*, *153*, 37–50. https://doi.org/10.1016/j.jconhyd.2013.07.005

Rasmussen, E. S., Dybkjær, K., & Piasecki, S. (2010). Lithostratigraphy of the Upper Oligocene–Miocene succession of Denmark. *Geological Survey of Denmark and Greenland Bulletin*, *22*, 1–92.

Rønde, V., McKnight, U. S., Sonne, A. T., Balbarini, N., Devlin, J. F., & Bjerg, P. L. (2017). Contaminant mass discharge to streams: Comparing direct groundwater velocity measurements and multi-level groundwater sampling with an in-stream approach. *Journal of Contaminant Hydrology*, *206*, 43–54. https://doi.org/10.1016/j.jconhyd.2017.09.010

Rubin, Y., & Hubbard, S. S. (2005). *Hydrogeophysics*. Dordrecht, the Netherlands: Springer.

Schwede, R. L., & Cirpka, O. A. (2010). Stochastic evaluation of mass discharge from pointlike concentration measurements. *Journal of Contaminant Hydrology*, *111*(1–4), 36–47. https://doi.org/10.1016/j.jconhyd.2009.10.011

Sonne, A. T., McKnight, U. S., Rønde, V., & Bjerg, P. L. (2017). Assessing the chemical contamination dynamics in a mixed land use stream system. *Water Research*, *125*, 141–151. https://doi.org/10.1016/j.watres.2017.08.031

Tarasov, A., & Titov, K. (2013). On the use of the Cole–Cole equations in spectral induced polarization. *Geophysical Journal International*, *195*(1), 352–356. https://doi.org/10.1093/gji/ggt251

Troldborg, M., Nowak, W., Lange, I. V., Pompeia Ramos dos Santos, M. C., Binning, P. J., & Bjerg, P. L. (2012). Application of Bayesian geostatistics for evaluation of mass discharge uncertainty at contaminated sites. *Water Resources Research*, *48*, W09535. https://doi.org/10.1029/2011WR011785

Troldborg, M., Nowak, W., Tuxen, N., Bjerg, P. L., Helmig, R., & Binning, P. J. (2010). Uncertainty evaluation of mass discharge estimates from a contaminated site using a fully Bayesian framework. *Water Resources Research*, *46*, W12552. https://doi.org/10.1029/2010WR009227

Weller, A., Slater, L., Binley, A., Nordsiek, S., & Xu, S. (2015). Permeability prediction based on induced polarization: Insights from measurements on sandstone and unconsolidated samples spanning a wide permeability range. *Geophysics*, *80*(2), D161–D173. https://doi.org/10.1190/geo2014-0368.1

Weller, A., Slater, L., & Nordsiek, S. (2013). On the relationship between induced polarization and surface conductivity: Implications for petrophysical interpretation of electrical measurements. *Geophysics*, *78*(5), D315–D325. https://doi.org/10.1190/geo2013-0076.1

Wemegah, D. D., Fiandaca, G., Auken, E., Menyeh, A., & Danuor, S. K. (2017). Spectral time-domain induced polarisation and magnetic surveying—An efficient tool for characterisation of solid waste deposits in developing countries. *Near Surface Geophysics*, *15*(1), 75–84.

Williams, K. H., Kemna, A., Wilkins, M. J., Druhan, J., Arntzen, E., N'Guessan, A. L., et al. (2009). Geophysical monitoring of coupled microbial and geochemical processes during stimulated subsurface bioremediation. *Environmental Science and Technology*, *43*(17), 6717–6723. https://doi.org/10.1021/es900855j